Solid State Sciences 14 (2012) 914–919

Contents lists available at SciVerse ScienceDirect

Solid State Sciences

journal homepage: www.elsevier.com/locate/ssscie

Indium oxide co-doped with tin and zinc: A simple route to highly conducting high density targets for TCO thin-film fabrication

I. Saadeddin [a,*], H.S. Hilal [a], R. Decourt [b], G. Campet [b], B. Pecquenard [b]

[a] College of Sciences, An-Najah National University, PO Box 7, Nablus, Palestine
[b] ICMCB, CNRS, Université Bordeaux 1, 87 avenue du Dr. A. Schweitzer, 33608 cedex, France

HIGHLIGHTS

- In_2O_3 based ceramic have been prepared without any hot or cold pressing techniques.
- A high density ceramic suitable for sputtering TCO thin films could be achieved.
- High solubility limit of Zn and Sn when co-doped into In_2O_3 bixbyte structure.
- A high conductivity ceramic (higher than ITO counterparts) was obtained.

GRAPHICAL ABSTRACT

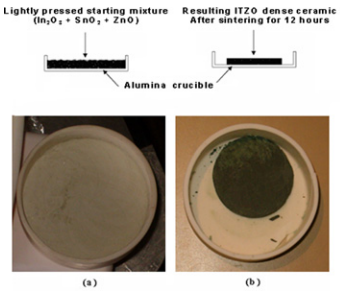

ARTICLE INFO

Article history:
Received 9 March 2012
Accepted 15 April 2012
Available online 28 April 2012

Keywords:
Co-doping
ITZO
Dense ceramic
Low resistivity

ABSTRACT

Indium oxide co-doped with tin and zinc (ITZO) ceramics have been successfully prepared by direct sintering of the powders mixture at 1300 °C. This allowed us to easily fabricate large highly dense target suitable for sputtering transparent conducting oxide (TCO) films, without using any cold or hot pressing techniques. Hence, the optimized ITZO ceramic reaches a high relative bulk density (~ 92% of In_2O_3 theoretical density) and higher than the well-known indium oxide doped with tin (ITO) prepared under similar conditions. All X-ray diagrams obtained for ITZO ceramics confirms a bixbyte structure typical for In_2O_3 only. This indicates a higher solubility limit of Sn and Zn when they are co-doped into In_2O_3 forming a solid-solution. A very low value of electrical resistivity is obtained for $[In_2O_3{:}Sn_{0.10}]{:}Zn_{0.10}$ (1.7×10^{-3} Ω cm, lower than ITO counterpart) which could be fabricated to high dense ceramic target suing pressure-less sintering.

© 2012 Elsevier Masson SAS. All rights reserved.

1. Introduction

Due to their unique transparent and conducting properties, indium tin oxide (ITO) thin films have been extensively studied for optoelectronic applications such as flat panel displays, organic light emitting diodes (OLEDs), etc. [1–5]. The ITO thin films are commonly deposited by magnetron sputtering using In_2O_3–SnO_2 mixture as the sputtering target [6]. The sputtering efficiency and properties of the sputtered films strongly depend on the characteristics of the sputtering targets (density, porosity, conductivity) [6,7]. Hence, dense targets increase the deposition rate and allow the deposition of homogeneous and dense thin films [8].

It is well-known that In_2O_3, SnO_2 and ITO suffers from a relative low bulk density (62–70%), even upon sintering at high temperatures (≥1350 °C) in air under normal atmospheric conditions [6,8–14]. However, very high density (97–99%) can be achieved for ITO and doped ITO, by sintering under hot isostatic pressure (HIP) [15]. Nevertheless, such sintering techniques are very expensive and not very convenient to prepare large area targets of defined shapes needed for industrial applications. Furthermore, it was reported that

* Corresponding author. Physics Department, An-Najah N. University, P.O.Box 7, Nablus, Palestine. Fax: +970 9 2345982.
E-mail address: iyadl2002@yahoo.com (I. Saadeddin).

1293-2558/$ – see front matter © 2012 Elsevier Masson SAS. All rights reserved.
doi:10.1016/j.solidstatesciences.2012.04.021

an addition of a few percent of dopant such as SiO_2, TiO_2, Bi_2O_3 or MgO to In_2O_3 or ITO increases the relative bulk density of the sintered materials (only cold pressed before sintering) up to ~ 93% [6–9,16,17]. As the additional oxide remains in the sintered ITO ceramics, it can have a negative effect on the optical properties of the sputtered films. However, the addition of ZnO into In_2O_3 and/or SnO_2 has no significant effect on the optical properties of the sputtered films [18–22]. Indeed, ZnO has a high optical band gap (~3.4 eV) and Zn^{2+} is a d^{10} element, like In^{3+}, with energy states that underlie the O^{2-}:$2p^6$ valence band of In_2O_3 [23]. The solubility limit of ZnO into In_2O_3 has been found by D. H. Park et al. to be ~1–2 mol % [24]. However, the solubility limit of Zn^{2+} into In_2O_3 ceramics was found to drastically increase up to 40 mol % when In^{3+} is co-substituted with equal amounts of Zn^{2+} and Sn^{4+} [25]. Unfortunately, the reported Zn^{2+}–Sn^{4+}co-substituted In_2O_3 ceramics were found to have low bulk density (≤60% of the theoretical density) and higher resistivities than their ITO analogues [25–27].

In this study, we report on the preparation and the physico-chemical characterization of ITZO ceramics having various compositions in comparison with ITO one. The nominal content of Sn^{4+} was fixed to 10 mol %, and the Zn^{2+} nominal content was varied from 0 to 10 mol %. According to literature, best electronic conductivity measurements have been obtained for In_2O_3 doped with an amount of Sn^{4+} that varies from ~6 to 10 mol % [28–34]. Our ultimate objective is to prepare high density and highly conductive large-scale targets usable for thin film deposition. To achieve this goal and to identify the optimum ceramic composition, all the phases have been carefully characterized in terms of their composition, density, structure as well as their electrical properties using various techniques.

2. Experimental

In_2O_3 (99.99%), SnO_2 (99.9%), and ZnO (99.9%) powders purchased from Aldrich, were used to prepare ITZO ceramics. Appropriate amounts of the selected oxides were ball milled for 30 min in an agate bowl containing agate balls and ethanol. The alcohol was then evaporated at 110 °C for 6 h. After drying, the powder was ground in an agate mortar, and filled in a 16 mm diameter cylindrical alumina crucible, and then 'hand-pressed' with a spatula. The mixed powder, filled in the crucible, was finally sintered at 1300 °C under air for 12 h. The chemical composition of the ceramic pellets was determined by Electron Probe X-ray Microanalysis (EPMA) using a CAMECA SX100 spectrometer. Thermo-gravimetric analysis (TGA) was recorded on a Setaram 24 setup from room temperature to 1300 °C, with a ramp of 5 °C/min. The dimensions of the resulting pellets were measured with a digital caliper vernier, and they were weighed using an analytical balance, in order to estimate the pellet bulk density. XRD data were acquired on a Philips PW1820 vertical goniometer in a Bragg Brentano geometry using CuKα radiation (λ = 1.5406 Å). The ceramic surfaces were observed by field emission scanning electron microscopy (FESEM) using a JEOL JSM-6700F microscope. Resistivity measurements were carried out as a function of the temperature, from 4.2 K to room temperature using a standard four probe configuration setup with direct current (home-made). Conduction band majority carrier (electrons) concentrations were determined from Seebeck coefficient measurements using a computerized home-made system.

3. Results and discussion

3.1. Chemical composition and bulk density

The EPMA results are reported in Table 1. For the sake of clarity, we have adopted a simplified sample identification scheme (Table 1) emphasizing the influence of Zn doping into ITO. These results show that there is a good agreement between the ceramic final compositions after sintering and the starting nominal composition. Only a slight loss of SnO_2 varying from ~ 0.5 to 1 mol % (which corresponds to ~0.27 to 0.54 weight %) is observed for both ITZO and ITO ceramics (Table 1) and confirmed by TGA analysis (Fig. 1). A low weight loss (0.28 weight % for [In_2O_3:$Sn_{0.10}$]:$Zn_{0.10}$ and 0.35 weight % for In_2O_3:$Sn_{0.10}$) occurs between 340 °C and 800 °C corresponding to Sn loss. Moreover, a weight loss (~0.6 weight %) is observed between room temperature and 340 °C which is related to the release of water (adsorbed water and water originating from hydroxyl groups). Finally, the slight weight loss measured for temperatures higher than 820 °C can be assigned for some oxygen loss. However, a small weight gain is observed, mainly for ITO, while cooling the ceramics, probably due to a partial oxygen uptake (Fig. 1).

The bulk density was found to increase from 2.52 to 6.57 g/cm^3 (reaching 92% of the In_2O_3 theoretical density), when the Zn content (y) increases from 0 to 10 mol % (Table 1). From Table 1 and Fig. 2, the highest density is reached for the co-doped ceramic for which the amount of Zn slightly overpasses that of Sn. The density enhancement must be correlated to the presence of Zn^{2+} in substitutional position as it occurred for AZTO ceramics [13], which leads to the formation of neutral oxygen vacancies (δ/2) according to:

$$In^{3+}_{2-x-y-\delta}Sn^{4+}_{x}Zn^{2+}_{y+\delta}O^{2-}_{3-(\delta/2)}\delta/2\left[\left(x-y\right)e^{-}_{C.B.}\right] \quad (1)$$

Indeed, the neutral oxygen vacancies promote mass transport at the grain boundary resulting in the facile densification of ceramic. However, the presence of Zn^{2+} in substitution position will compensate for the free carriers produced by doping with Sn^{4+} [according to formula (1)] resulting in net charge content per formula unit equal to "$x-y$".

3.2. Structure and morphology

3.2.1. ITO (In_2O_3:Sn)

X-Ray Diffraction patterns for In_2O_3 and ITO (In_2O_3:$Sn_{0.10}$ nominal composition) powders annealed at 1300 °C are shown in Fig. 3. For ITO, some extra low intensity peaks corresponding to the

Table 1
Ceramic chemical composition and bulk density for [In_2O_3:$Sn_{0.10}$]:Zn_y ceramics (ITZO), $0 \le y \le 0.10$. The reported bulk densities were deduced by measuring pellet dimensions and weights. Note that the pellets are prepared by 'hand-pressing' powders mixture in an alumina crucible. δ/2 indicates the neutral oxygen vacancy created by doping with Zn, the value of δ/2 varying with Zn content.

Sample identification	Starting mixture	Ceramic composition determined by EPMA ± 5%	Bulk density (g/cm^3) ± 0.05
In_2O_3:$Sn_{0.10}$ (ITO)	$(In_2O_3)_{0.95}$+$(SnO_2)_{0.1}$	$In_{1.910}Sn_{0.090}O_3$	2.52
[In_2O_3:$Sn_{0.10}$]:$Zn_{0.04}$	[$(In_2O_3)_{0.95}$+$(SnO_2)_{0.1}$]$_{0.98}$+$(ZnO)_{0.04}$	$In_{1.866}Sn_{0.089}Zn_{0.045}O_{3-\delta/2}$	3.50
[In_2O_3:$Sn_{0.10}$]:$Zn_{0.06}$	[$(In_2O_3)_{0.95}$+$(SnO_2)_{0.1}$]$_{0.97}$+$(ZnO)_{0.06}$	$In_{1.847}Sn_{0.091}Zn_{0.063}O_{3-\delta/2}$	3.92
[In_2O_3:$Sn_{0.10}$]:$Zn_{0.08}$	[$(In_2O_3)_{0.95}$+$(SnO_2)_{0.1}$]$_{0.96}$+$(ZnO)_{0.08}$	$In_{1.827}Sn_{0.090}Zn_{0.083}O_{3-\delta/2}$	4.87
[In_2O_3:$Sn_{0.10}$]:$Zn_{0.10}$	[$(In_2O_3)_{0.95}$+$(SnO_2)_{0.1}$]$_{0.95}$+$(ZnO)_{0.10}$	$In_{1.812}Sn_{0.090}Zn_{0.098}O_{3-\delta/2}$	6.57

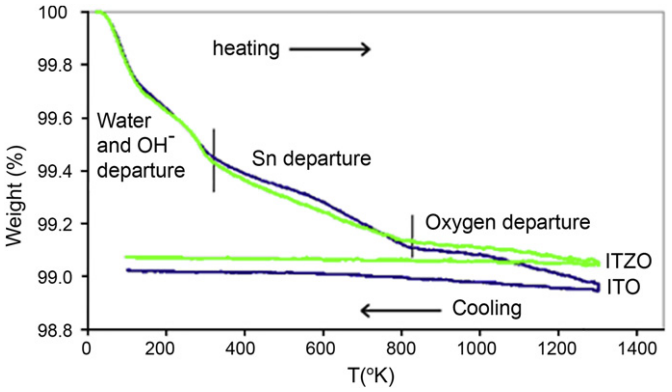

Fig. 1. TGA data for In_2O_3:$Sn_{0.10}$ (ITO) and [In_2O_3:$Sn_{0.10}$]:$Zn_{0.10}$ (ITZO) (nominal composition).

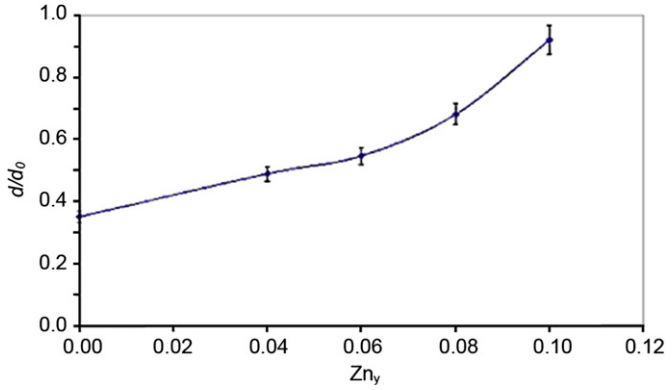

Fig. 2. Relative bulk density (d/d_0) evolution with Zn_y for [In_2O_3:$Sn_{0.10}$]:Zn_y ceramics.

rutile SnO_2 are observed in addition to the peaks characteristic of the bixbyite structure (JCPDS reference pattern no. 89-4596). The ratio between the highest intensity ITO peak and the highest intensity SnO_2 peak is 1/0.03. This results is in good accordance with the solubility limit of SnO_2 into In_2O_3 at 1300 °C which reaches 6 mol % as indicated by Enoki et al. [34]. In addition, a pronounced decrease of the peaks FWHM (full width at half maximum) for ITO

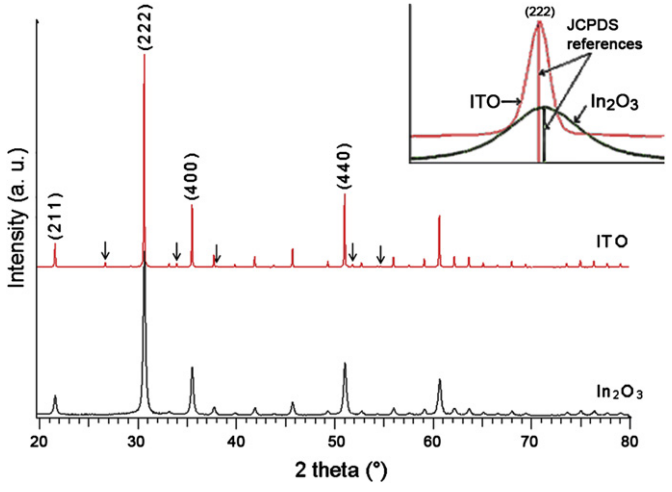

Fig. 3. XRD data for (a) undoped In_2O_3 and (b) In_2O_3:$Sn_{0.01}$ (ITO) powders annealed at 1300 °C. The shift of the ITO (222) peak is shown in the insert. (↓) indicates peaks which correspond to the rutile SnO_2.

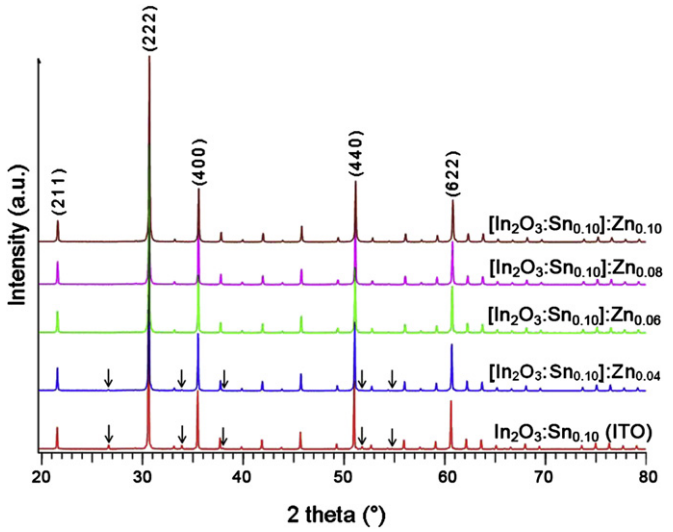

Fig. 4. XRD diagrams for ITZO sintered powders having the nominal composition [In_2O_3:$Sn_{0.10}$]:Zn_y, $0 \le y \le 0.10$. (↓) indicates peaks which correspond to the rutile SnO_2 structure.

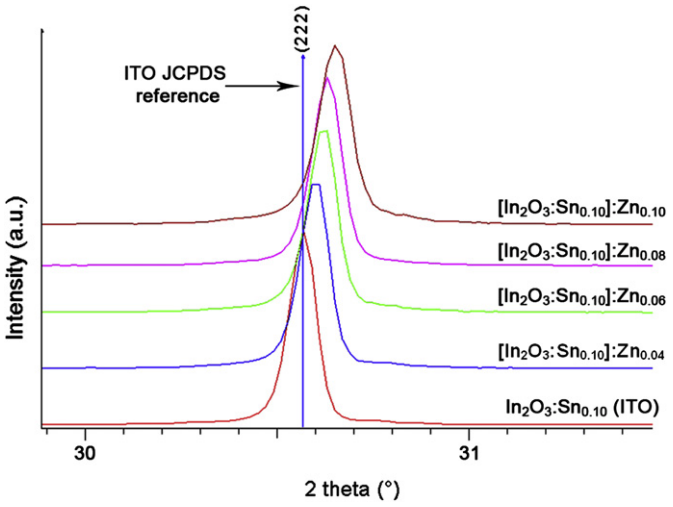

Fig. 5. The shift of the X-ray (222) peak for ITZO sintered powders in comparison with ITO counterpart (JCPDS reference pattern 89-4596).

powder compared to In_2O_3 (JCPDS reference pattern no. 71-2194) is observed, indicating an enhancement of the crystallinity for doped In_2O_3. For example, if we consider the (222) peak, which is the most intense peak, the FWHM was found to decrease from 0.278° for In_2O_3 to 0.083° for ITO, showing an enhancement of the crystallite size. Finally, we have noticed a slight shift of the main diffraction peaks of ITO towards lower angles compared to pure In_2O_3 (Fig. 4), which accounts for a slight increase of the unit cell parameter from

Table 2
Cell parameter evolution with Zn content for ITZO sintered powders. ITO cell parameter is added as a reference.

Sample identification	a (Å) ± 0.002
In_2O_3:$Sn_{0.10}$ (ITO)	10.123
[In_2O_3:$Sn_{0.10}$]:$Zn_{0.04}$	10.114
[In_2O_3:$Sn_{0.10}$]:$Zn_{0.06}$	10.107
[In_2O_3:$Sn_{0.10}$]:$Zn_{0.08}$	10.104
[In_2O_3:$Sn_{0.10}$]:$Zn_{0.10}$	10.097

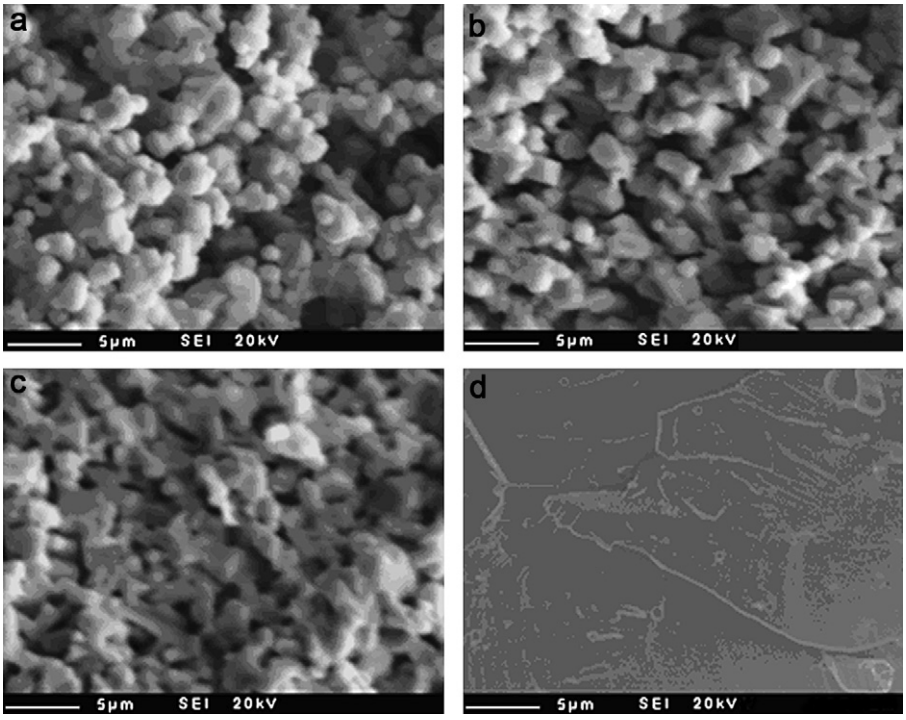

Fig. 6. SEM micrographs for ceramics having the following nominal compositions (a) In_2O_3:$Sn_{0.10}$, (b) [In_2O_3:$Sn_{0.10}$]:$Zn_{0.04}$, (c) [In_2O_3:$Sn_{0.10}$]:$Zn_{0.08}$, and (d) [In_2O_3:$Sn_{0.10}$]:$Zn_{0.10}$.

10.117 Å for In_2O_3 to 10.123 Å for ITO. This behavior is not expected if we consider the substitution of a part of In^{3+} by Sn^{4+} because Sn^{4+} has an ionic radius (0.69 Å) which is smaller than In^{3+} (0.80 Å) [35]. Thus, the enhancement of the cell parameter along with the decrease of the peaks FWHM, could be related to the high electronic carrier concentration in the conduction band for ITO originating from Sn^{4+} in cationic-substitution positions (rather than from Sn^{4+} in interstitial positions) [23].

3.2.2. ITZO (In_2O_3:Sn:Zn)

XRD patterns for ITZO powders annealed at 1300 °C (Fig. 4) show that they are very well crystallized and adopted the bixbyite structure. No Extra peaks corresponding to ZnO_x or $Zn_kIn_2O_{3+k}$ structures are observed while increasing Zn content up to 10 mol %. Moreover, the minor peaks characteristic of SnO_2 structure observed with those of ITO structure are found to gradually vanish with increasing Zn content and totally absent for Zn content higher than 6 mol %. These results confirms the increase of solubility for both Zn and Sn when they are co-doped into In_2O_3 [25]. Indeed, the increase of the solubility is attributed to the possible isovalent substitution of two In^{3+} by one Zn^{2+} and one Sn^{4+}. A shift of the main diffraction peaks towards higher angle occurring when Zn content rises (Fig. 5), accounts for a decrease of the 'a' lattice parameter (Table 2). This could be attributed to the existence of Zn^{2+} in substitutional positions as we have already suggested in formula (1) ($In^{3+}_{2-x-y-\delta}Sn^{4+}_xZn^{2+}_{y+\delta}O^{2-}_{3-(\delta/2)}\ _{\delta/2}\ [(x-y)e^-_{C.B.}]$). Indeed, the 6-fold coordinated Zn^{2+} has an ionic radius (0.74 Å) which is smaller than that of In^{3+} (0.80 Å) [35].

The evolution of the morphology of ceramic surface with Zn content is presented on the SEM micrographs (Fig. 6). The SEM images clearly show that as Zn content increases in the ceramic, the grain percolation increases and porosity decreases. This confirms the gradual increase of density with Zn content (see Table 1 and

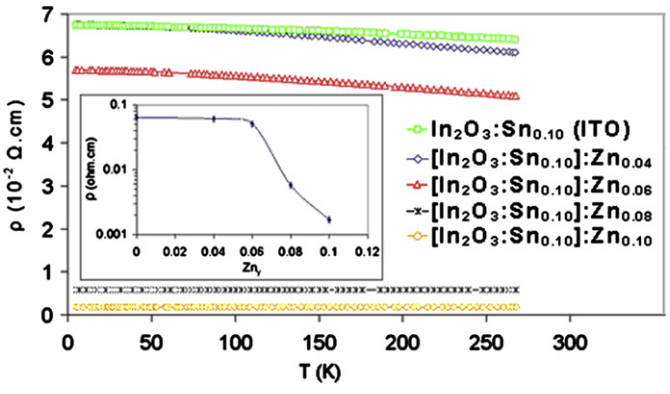

Fig. 7. Resistivity evolution with temperature for different ITZO ceramics having a nominal Zn contents varying from 0 to 0.10. The resistivity evolution with Zn content is shown in the insert at room temperature.

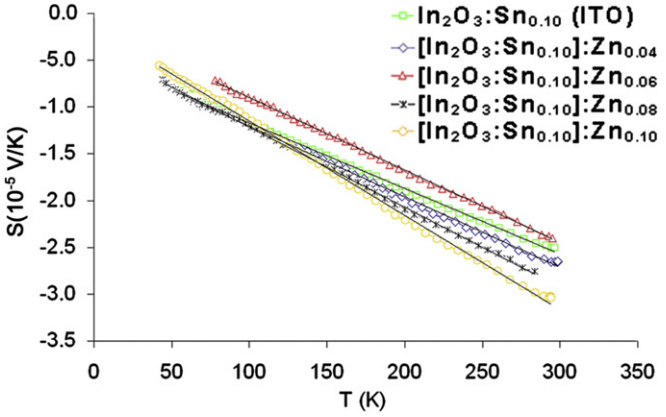

Fig. 8. Seebeck coefficient evolution with temperature for various ITZO ceramics ([In_2O_3:$Sn_{0.10}$]:Zn_y). The nominal Zn content was varied from 0 to 0.10.

Table 3
E_F–E_C, mobility, carrier concentration and resistivity values for ITO and different ITZO ceramics. The carrier concentration was deduced using Seebeck coefficient measurements.

Sample identification	E_F–E_C (eV)	Carrier mobility ($cm^2V^{-1}\ s^{-1}$) ± 5%	Carrier concentration ($10^{20}\ e^-\ cm^{-3}$) ± 5%	Resistivity ($10^{-3}\ \Omega$ cm) ± 5%
In_2O_3:$Sn_{0.10}$ (ITO)	0.67	0.16	6.30	64.0
[In_2O_3:$Sn_{0.10}$]:$Zn_{0.04}$	0.62	0.18	5.63	61.0
[In_2O_3:$Sn_{0.10}$]:$Zn_{0.06}$	0.61	0.23	5.42	51.0
[In_2O_3:$Sn_{0.10}$]:$Zn_{0.08}$	0.55	2.30	4.68	5.8
[In_2O_3:$Sn_{0.10}$]:$Zn_{0.10}$	0.47	10.09	3.65	1.7

Table 4
ITZO parameters and final compositions calculated using EPMA results and carrier concentration determined by Seebeck measurements.

Sample identification	x	y	δ	Final formula
[In_2O_3:$Sn_{0.10}$]:$Zn_{0.06}$	0.091	0.057	0.006	$In^{3+}_{1.847}Sn^{4+}_{0.091}Zn^{2+}_{0.063}O^{2-}_{2.997\ 0.003}[(0.034)e^-_{C.B.}]$
[In_2O_3:$Sn_{0.10}$]:$Zn_{0.08}$	0.092	0.062	0.020	$In^{3+}_{1.826}Sn^{4+}_{0.092}Zn^{2+}_{0.082}O^{2-}_{2.990\ 0.010}[(0.030)e^-_{C.B.}]$
[In_2O_3:$Sn_{0.10}$]:$Zn_{0.10}$	0.090	0.066	0.032	$In^{3+}_{1.812}Sn^{4+}_{0.090}Zn^{2+}_{0.098}O^{2-}_{2.984\ 0.016}[(0.024)e^-_{C.B.}]$

Fig. 2). The highest density (~6.57 g/cm^3) was observed for the ceramic of composition $In_{1.812}Sn_{0.090}Zn_{0.098}O_{3-\delta/2}$ corresponding to the nominal composition ([In_2O_3:$Sn_{0.10}$]:$Zn_{0.10}$, see Table 1) which has almost a complete grain percolation (Fig. 6 (d)). As we have previously explained, co-doping In_2O_3 with Zn and Sn leads to the presence of neutral oxygen vacancies (δ/2) according to formula (1); that allows mass transfer at the grain boundaries and hence grain percolation, leading to an enhancement of the ceramic density [13].

3.3. Electrical properties

ITZO ceramics exhibited lower electrical resistivities than ITO one (Fig. 7), prepared using the same procedure described above. Between 0 and 6 mol % of Zn, only a minor decay is observed whereas the resistivity drastically decreases for higher Zn contents reaching a minimum value (~$1.7 \times 10^{-3}\ \Omega$ cm) for the ceramic that nominally contains 10 mol % of Zn. It is striking that the lowest resistivity is achieved for the ceramic that has the highest density. The three ceramics having the highest resistivities (Fig. 7) are characterized by a semiconducting behavior, which could as well be related to the low density reported above for these ceramics (Table 1) while the others have a metallic behavior. Indeed, the low density of these ceramics will be responsible for their low electron-carrier mobility arising from electron scattering at grain boundary and/or voids.

The ceramic carrier mobility was deduced from the resistivity and carrier concentration from Seebeck measurements versus temperature (Fig. 8). We have first deduced the energy difference between the conduction band and the Fermi energy level $|E_F–E_C|$ from the slope of the linear graphs (Fig. 8), using the following equation:

$$S \approx -\frac{k_B}{e}\frac{\pi^2}{|E_F - E_C|}k_B T \quad (2)$$

where S is the Seebeck coefficient expressed in V/K. The carrier concentration can then be deduced using the following equation for a degenerate semiconductor:

$$E_F - E_C = \frac{h^2}{2m^*}\left(\frac{3N}{8\pi}\right)^{2/3} \quad (3)$$

where N is the carrier concentration, and m^* is the electron effective mass (assuming m^* is equal to 0.4 m_e [36]). Afterwards, the carrier mobility could be assessed. These electrical data deduced from Seebeck and resistivity measurements are listed in Table 3. First, the carrier concentration decreases with Zn amount in the ceramic. This can be explained by the increasing substitution of In^{3+} by Zn^{2+} in the In_2O_3 structure, which is confirmed by the shift towards higher angle of the different peaks on the XRD diagrams (Fig. 5). As expected, a strong enhancement of the carrier mobility is confirmed for high Zn content. Indeed, the enhancement of the mobility must be correlated to the strong enhancement of the grain percolation (Fig. 6).

Using EPMA results and electrical measurements, we can deduce the accurate composition for the ITO and ITZO ceramics including the amount of oxygen vacancies. In the case of ITO ceramic, we have only a substitution of In^{3+} by Sn^{4+} in the In_2O_3 lattice producing free electron carriers in the conduction band according to:

$$In^{3+}_{2-x}Sn^{4+}_x O^{2-}_3\left[xe^-_{C.B.}\right] \quad (4)$$

x was deduced from the carrier concentration (Table 3) and found to be equal to ~0.04 per formula unit. Hence, one should normally write the following formula for ITO:

$$In^{3+}_{1.96}Sn^{4+}_{0.04}O^{2-}_3\left[0.04e^-_{C.B.}\right] \quad (5)$$

However, formula (5) differs from that determined using EPMA: $In_{1.91}Sn_{0.09}O_3$ which is more accurate. In fact, let us recall that the 0.09 Sn content is divided into three parts: (i) a part goes to form the rutile SnO_2 additional phase as previously shown by XRD analysis, (ii) another part substitutes In^{3+} producing free electrons in the conduction band according to formula (5), and (iii) the remaining Sn are most probably segregated at the grain boundaries where structural disorder predominates. For ITZO, both Sn^{4+} and Zn^{2+} substitute In^{3+} in the In_2O_3 according to formula (1) ($In^{3+}_{2-x-y-\delta}Sn^{4+}_x Zn^{2+}_{y+\delta}O^{2-}_{3-(\delta/2)\ \delta/2}[(x-y)e^-_{C.B.}]$). The calculated parameters (x, y and δ) and the corresponding final composition for the most conducting ITZO ceramic are listed in Table 4.

4. Conclusion

We have prepared ITZO ceramics by fixing Sn content to 10 mol % and varying the Zn content from 0 to 10 mol %. These doping levels were chosen in order to remain in the solid-solution region of the In_2O_3 bixbyite structure and, thereby, avoid the formation of any additional phase. For the nominal composition ([In_2O_3:$Sn_{0.10}$]:$Zn_{0.10}$), the density is high, reaching 92% of In_2O_3 theoretical density. The lowest resistivity ($1.7 \times 10^{-3}\ \Omega$ cm) was also obtained for this dense ceramic. In summary, co-doping In_2O_3 with Sn^{4+} and Zn^{2+}, forming ITZO ceramic ([In_2O_3:Sn]:Zn), allowed

us to achieve a simple and straightforward target preparation by direct sintering the 'hand-pressed' powder mixture in an appropriate alumina crucible, without using any cold or hot pressing procedure. This will markedly reduce the manufacturing cost of commercial ITO based targets and particularly of large area targets intended for industrial thin film coatings. The preliminary optical and electrical properties obtained on relative thin films are very promising, even on flexible polymer substrates, and will be reported in the near future.

Acknowledgments

The authors gratefully acknowledge the contribution of M. Lahaye and E. Sellier in offering technical help and valuable suggestions concerning EPMA measurements and SEM analysis. Acknowledgment is also conducted to Prof. M. Subramanian for the helpful review for this manuscript. Acknowledgment is also conducted to The financial support by the French ministry of foreign affairs. Partial financial support from French-Palestine cooperation Project (Al-Maqdisi) is also acknowledged.

References

[1] J.J. Vossen, Phys. Thin Films 9 (1977) 1.
[2] N. Balasubramanian, A. Subrahamanyam, J. Electrochem. Soc. 138 (1991) 322.
[3] I. Hamberg, C.G. Granqvist, J. Appl. Phys. 60 (1986) R123.
[4] C.W. Tang, S.A. Van Slyke, Appl. Phys. Lett. 51 (1987) 913.
[5] I. Hamberg, A. Hjortsberg, C. Granqvist, Appl. Phys. Lett. 40 (1982) 362.
[6] N. Nadaud, M. Nanot, P. Boch, J. Am. Ceram. Soc. 77 (1994) 843.
[7] B.L. Gehman, S. Jonsson, T. Rudolph, M. Scherer, M. Weight, R. Werner, Thin Solid Films 220 (1992) 333.
[8] T. Vojnovich, R.J. Bartton, Ceram. Bull. 54 (1992) 216.
[9] J.L. Bates, C.W. Griffin, D.D. Marchant, J.E. Gernier, Am. Ceram. Soc. Bull. 65 (1996) 673.
[10] H. Watanabe, New Ceram. 4 (1996) 19.
[11] Y. Kojima, New Ceram. 12 (1992) 47.
[12] J.H.W. de Wit, J. Solid State Chem. 13 (1975) 192.
[13] I. Saadeddin, H.S. Hilal, B. Pecquenard, J. Marcus, A. Mansouri, C. Labrugere, M.A. Subramanian, G. Campet, Solid State Sci. 8 (2006) 7.
[14] E.R. Leite, J.A. Cerri, E. Longo, J.A. Varela, C.A. Paskocima, J. Eur. Cer. Soc. 21 (2001) 669.
[15] S. Martin, K. Matrin, D. Wolfgang, G. Gruce, U.S. Patent 553, 1948, 1996.
[16] T. Nate, T. Kishi, Hyomen-Gijyutu 43 (1992) 20.
[17] M. Suzuki, M. Muraoka, Y. Sawada, J. Matsushita, Mater. Sci. Eng. B 54 (1998) 46.
[18] E. Fortunato, A. Pimentel, A. Gonçalves, A. Marques, R. Martins, Thin Solid Films 502 (2006) 104.
[19] T. Minami, T. Kakumu, Y. Takeda, S. Takata, Thin Solid Films 290-291 (1996) 1.
[20] N. Naghavi, A. Rougier, C. Marcel, C. Guéry, J.B. Leriche, J.M. Tarascon, Thin Solid Films 360 (2000) 233.
[21] T. Minami, T. Yamamoto, Y. Toda, T. Miyata, Thin Solid Films 373 (2000) 189.
[22] I. Saadeddin, B. Pecquenard, J.P. Manaud, R. Decourt, C. Labrugère, T. Buffeteau, G. Campet, Appl. Surf. Sci. 253 (2007) 5240.
[23] I. Saadeddin, Ph.D. Thesis, Bordeaux 1 University, Bordeaux, France (2007).
[24] D.H. Park, K.Y. Son, J.H. Lee, J.J. Kim, J.S. Lee, Solid State Ionics 172 (2004) 431.
[25] G.B. Palmer, K.R. Poeppelmeier, T.O. Mason, Chem. Mater. 9 (1997) 3121.
[26] A. Ambrosini, G.B. Palmer, A. Maignan, K.R. Poeppelmeier, M.A. Lane, P. Brazis, C.R. Kannewurf, T. Hogan, T.O. Mason, Chem. Mater. 14 (2002) 52.
[27] A. Ambrosini, S. Malo, K.R. Poeppelmeier, M.A. Lane, C.R. Kannewurf, T.O. Mason, Chem. Mater. 14 (2002) 58.
[28] J.C.C. Fan, J.B. Goodenough, J. Appl. Phys. 48 (1977) 3524.
[29] T. Minami, T. Kakumu, K. Shimokawa, S. Takata, Thin Solid Films 317 (1998) 318.
[30] M. Russak, J. De Carlo, J. Vac. Sci. Technol. 1 (1983) 1563.
[31] H. Kim, A. Piqué, J.S. Horwitz, H. Mattoussi, H. Murata, Z.H. Kafafi, D.B. Chrisey, Appl. Phys. Lett. 74 (1999) 3444.
[32] T.O. Mason, a G.B. González, a J.-H. Hwangb, D.R. Kammler, Phys. Chem. Chem. Phys. 5 (2003) 2183.
[33] H. Kim, C.M. Gilmore, J. Appl. Phys. 86 (1999) 6451.
[34] H. Enoki, J. Echogoya, H. suto, J. Mater. Sci. 26 (1991) 4110.
[35] R.D. Shannon, Acta Cryst. A 32 (1976) 751.
[36] C. Marcel, Ph.D. thesis, Bordeaux 1 University, Bordeaux, France (1998).